

Thermal lattice Boltzmann method for multiphase flowsAlexander L. Kupershtokh,¹ Dmitry A. Medvedev,^{1,2,*} and Igor I. Griбанov¹¹*Lavrentyev Institute of Hydrodynamics, Siberian Branch of Russian Academy of Sciences, Lavrentyev prosp. 15, 630090 Novosibirsk, Russia*²*Novosibirsk State University, Pirogova str. 2, 630090 Novosibirsk, Russia*

(Received 23 October 2017; revised manuscript received 21 June 2018; published 24 August 2018)

An alternative method to simulate heat transport in the multiphase lattice Boltzmann (LB) method is proposed. To solve the energy transport equation when phase boundaries are present, the method of a passive scalar is considerably modified. The internal energy is represented by an additional set of distribution functions, which evolve according to an LB-like equation simulating the transport of a passive scalar. Parasitic heat diffusion near boundaries with a large density gradient is suppressed by using special “pseudoforces” which prevent the spreading of energy. The compression work and heat diffusion are calculated by finite differences. A new method to take into account the latent heat of a phase transition $Q(T)$ is realized. The latent heat is released or absorbed continuously inside a thin transition layer in a certain range of density, $\rho_1 < \rho < \rho_2$. This allows one to avoid interface tracking. Several tests were carried out concerning all aspects of the processes. It is shown that the Galilean invariance and the scaling of the thermal conduction process hold, as well as the correct dependence of the sound speed on the heat capacity ratio. The method proposed has low scheme diffusion of the internal energy, and it can be applied to modeling a wide range of multiphase flows with heat and mass transfer even for high density ratios of liquid and vapor phases.

DOI: [10.1103/PhysRevE.98.023308](https://doi.org/10.1103/PhysRevE.98.023308)**I. INTRODUCTION**

Simulation of fluid flows with phase transitions between liquid and vapor is difficult because new phase boundaries can appear in the bulk during calculations, and the existing boundaries can disappear or change in topology. Therefore, the application of interface tracking methods is difficult if at all possible. Moreover, the density ratio of liquid and vapor phases is usually high (reaching tens and hundreds of thousands), leading to noticeable numerical diffusion and/or dispersion near the boundaries when using Eulerian finite-difference methods.

The lattice Boltzmann method (LBM) [1,2] is based on the solution of a kinetic equation for pseudoparticles. It was widely applied for simulating flows of single-phase and multiphase media [3–10]. Moreover, the method is easily parallelizable on graphic accelerators using CUDA technology [8–14].

However, the simulation of heat transport in the LBM is a problem which has not been fully solved till now. Several essentially different approaches have been proposed. The first approach uses an extended set of lattice Boltzmann equation (LBE) velocities [15–18]. The second group is finite-difference Euler methods for the energy equation [19]. The third method is based on the idea that heat is transferred to neighboring nodes in accordance with the portions of “LBE particles” that move in each direction. The fourth method is based on an additional set of distribution functions for the thermal energy equation (“passive scalar” method) [20,21].

The first approach has a rather narrow range of simulated temperatures where simulations are stable, and the amount of

data increases significantly. This method was applied only to single-phase flows. The latter three methods were compared in simulations of one-dimensional (1D) uniform flow with some passive scalar that should move with the fluid [22].

When the energy equation is solved by finite-difference Euler methods, large numeric diffusion arises. Moreover, the diffusivity depends on the velocity of the fluid. This restricts the possibility of modeling significantly.

The method of heat transfer to neighboring nodes with LBE particles has a constant but high numerical diffusivity.

The passive scalar approach is realized in the LBM by introducing an additional set of distribution functions for the energy equation. This model has much lower numeric diffusion than other methods. This method is usually used for single-phase flows for which the density of the fluid is almost constant. In this case, the energy equation can be written in terms of the temperature T , which can be considered as the passive scalar [20,21,23]. This approach was used for the simulation of melting and solidification processes with conductive and convective heat transport also for the case of a constant density and heat capacity [24–27]. However, the transport of internal energy should be considered instead of the temperature if a liquid-vapor phase transition is present and the change in density is not small. This approach was used in Refs. [21,28] and it was combined with an extended velocity set in Ref. [29]. Nevertheless, only single-phase flows were considered in these works. The main problem is that, except for numerical diffusivity, there exists a parasitic dispersion (spreading) of energy at liquid-vapor interfaces [30]. In Ref. [31], a correction term was added to the evolution equation for the second set of distribution functions. Unfortunately, this approach is valid only for fluids at rest and is not suitable for moving fluids.

*dmedv@hydro.nsc.ru

In this paper, we give the solutions of these difficulties for multiphase flows. To exclude parasitic numerical diffusion, we propose the introduction of special “pseudoforces” for the energy distribution functions [30]. As a result, our method is valid for moving two-phase flows.

II. LATTICE BOLTZMANN METHOD

The lattice Boltzmann method is based on the solution of a kinetic equation for pseudoparticles. Only a limited set of particle velocities \mathbf{c}_k is possible such that the vectors $\mathbf{e}_k = \mathbf{c}_k \Delta t$ correspond to vectors to neighboring nodes on a regular spatial lattice [32]. The usual choice of velocity set is 3 vectors in the 1D case (D1Q3 model, $|\mathbf{c}_k| = 0, h/\Delta t$), 9 velocities in the 2D case (D2Q9, $|\mathbf{c}_k| = 0, h/\Delta t, \sqrt{2}h/\Delta t$), and 19 velocities in the 3D case (D3Q19, $|\mathbf{c}_k| = 0, h/\Delta t, \sqrt{2}h/\Delta t$). Here, h is the lattice space, and Δt is the time step.

One-particle distribution functions N_k are used as main variables; they have the meaning of parts of the fluid density at a node. The evolution equation for N_k has the form

$$\begin{aligned} N_k(\mathbf{x} + \mathbf{c}_k \Delta t, t + \Delta t) \\ = N_k(\mathbf{x}, t) + \Omega_k(N) + \Delta N_k, \quad k = 0, \dots, b, \end{aligned} \quad (1)$$

where Ω_k is the collision operator, and ΔN_k is the change of distribution functions under the action of volume forces (both external and internal).

The collision operator is mostly chosen in the form of a relaxation to local equilibrium with one (Bhatnagar-Gross-Krook (BGK) model [32]) or several (multi-relaxation-time model [33]) relaxation times. For the BGK model, the collision operator is

$$\Omega_k = \frac{N_k^{\text{eq}}(\rho, \mathbf{u}) - N_k(\mathbf{x}, t)}{\tau},$$

where $\tau = t_{\text{rel}}/\Delta t$ is the nondimensional relaxation time. Equilibrium distribution functions are usually taken as truncated Maxwellians up to second order in the fluid velocity \mathbf{u} [34]:

$$N_k^{\text{eq}}(\rho, \mathbf{u}) = \rho w_k \left(1 + \frac{(\mathbf{c}_k \cdot \mathbf{u})}{\theta} + \frac{(\mathbf{c}_k \cdot \mathbf{u})^2}{2\theta^2} - \frac{\mathbf{u}^2}{2\theta} \right). \quad (2)$$

Coefficients w_k depend on the lattice geometry [32]. They are $w_0 = 2/3$, $w_{1,2} = 1/6$ for the 1D model D1Q3, $w_0 = 4/9$, $w_{1-4} = 1/9$, $w_{5-9} = 1/36$ for the 2D model D2Q9, and $w_0 = 1/3$, $w_{1-6} = 1/18$, $w_{7-18} = 1/36$ for the 3D model D3Q19. The kinetic temperature of pseudoparticles in lattice Boltzmann (LB) models listed is $\theta = (h/\Delta t)^2/3$, and the kinematic viscosity is defined by the relaxation time $\nu = \theta(\tau - 1/2)\Delta t$. The change of distribution functions at a node due to the action of a total force \mathbf{F} is calculated using the exact difference method (EDM) [35,36],

$$\Delta N_k(\mathbf{x}, t) = N_k^{\text{eq}}(\rho, \mathbf{u} + \Delta \mathbf{u}) - N_k^{\text{eq}}(\rho, \mathbf{u}), \quad (3)$$

where $\Delta \mathbf{u} = \mathbf{F}\Delta t/\rho$ is the change in the fluid velocity in one time step.

The density ρ and velocity \mathbf{u} of the fluid are calculated as

$$\rho = \sum_{k=0}^b N_k, \quad \rho \mathbf{u} = \sum_{k=1}^b \mathbf{c}_k N_k. \quad (4)$$

Under the action of volume forces, the physical fluid velocity \mathbf{u}^* should be defined at half-time step [37],

$$\rho \mathbf{u}^* = \sum_{k=1}^b \mathbf{c}_k N_k + \mathbf{F}\Delta t/2. \quad (5)$$

III. PHASE TRANSITIONS

In order to simulate phase transitions in a fluid, it is necessary to model in the LBM the attractive part of the “intermolecular” interaction. This was done in Ref. [5] by the introduction of attractive forces acting on the fluid at a node from neighboring nodes. Later, the total force \mathbf{F} acting on the fluid at a node was introduced as a gradient of the pseudopotential U defined using the equation of state for the fluid [6,19]

$$\mathbf{F} = -\nabla U = -\nabla(p(\rho, T) - \rho\theta). \quad (6)$$

The LBM with such attractive forces represents a phase boundary as a thin transition layer between liquid and vapor where the density changes smoothly across several lattice nodes (interface capturing). In this case, the surface tension arises at phase boundaries.

In Ref. [38], we proposed the introduction of a new function, $\Phi = \sqrt{-U}$. Equation (6) can be rewritten in the equivalent form

$$\mathbf{F} = \nabla(\Phi^2) \equiv 2\Phi\nabla\Phi. \quad (7)$$

These two mathematically equivalent expressions can be discretized differently, and a generalized form was proposed in [39]:

$$\mathbf{F}_N = 2A\nabla(\Phi^2) + (1 - 2A)2\Phi\nabla\Phi. \quad (8)$$

Here, A is a free parameter which allows one to minimize the numerical errors in phase densities at the coexistence curve.

A sufficiently isotropic approximation of formula (9) is

$$\begin{aligned} \mathbf{F}(\mathbf{x}) = \frac{1}{\alpha h} \left[A \sum_{k=1}^b G_k \Phi^2(\mathbf{x} + \mathbf{e}_k) \mathbf{e}_k \right. \\ \left. + (1 - 2A)\Phi(\mathbf{x}) \sum_{k=1}^b G_k \Phi(\mathbf{x} + \mathbf{e}_k) \mathbf{e}_k \right], \end{aligned} \quad (9)$$

where coefficients $G_k > 0$ differ for different lattice directions. For neighbor nodes, they are $G_k = 1$. For next-neighbor nodes, the values of the coefficients ensuring isotropy are $G_{5-8} = 1/4$ for the 2D model D2Q9 and $G_{7-18} = 1/2$ for the 3D model D3Q19. The coefficients α are equal to 1, 3/2, and 3 for models D1Q3, D2Q9, and D3Q19, respectively.

The so-called “combined” approximation, (9), becomes a “local” approximation for $A = 0$ and a “mean-value” approximation for $A = 0.5$ [38–40]. This “combined” approximation was compared in [38–40] with the “local” and “mean-value” approximations. The LBM simulations are more stable for the combined approximation, which allows one to reach density ratio values of up to 10^6 for a quasistationary flat liquid-vapor interface.

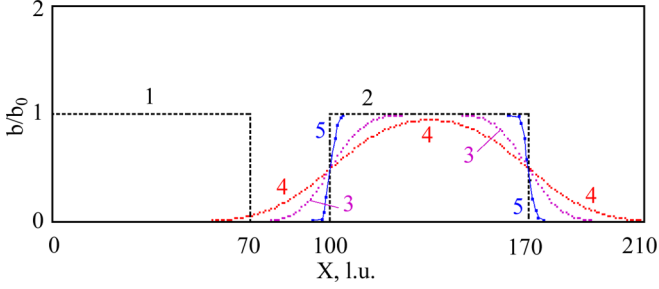


FIG. 1. Numerical diffusivity of a relative concentration b/b_0 of the passive scalar in a 1D liquid flow of constant density for the case of zero diffusion [22]. The velocity of uniform flow is $u = 0.1h/\Delta t$. Curves show the initial distribution of the scalar at $t = 0$ (curve 1); theoretical scalar distribution without diffusion at $t = 1000$ (curve 2); finite-difference method, $D_1 = 0.045h^2/\Delta t$ (curve 3); method of “LBE particles,” $D_2 = h^2/6\Delta t$ (curve 4); and standard method of an additional LBE component, $D_3 = 0.0033h^2/\Delta t$ (curve 5).

In the present work, we used the van der Waals equation of state, which is written in reduced variables as

$$\tilde{p} = \frac{8\tilde{\rho}\tilde{T}}{3 - \tilde{\rho}} - 3\tilde{\rho}^2.$$

Here and below, the pressure, density, and temperature are scaled by their values at the critical point, $\tilde{p} = p/p_c$, $\tilde{\rho} = \rho/\rho_c$, $\tilde{T} = T/T_c$. For this equation of state, approximation (9) gives the best agreement with the phase coexistence curve at $A = -0.152$ (in simulations the deviation of density from the theoretical value is less than 0.4% in the range of temperature from the critical one $\tilde{T} = 1$ down to $\tilde{T} = 0.4$ [38]). More complex equations of state including tabulated ones for real fluids are considered in [40,41].

The stability of the LBM with the equation of state in the form $p = p(\rho, T)$ is defined by the criterion [36]

$$\left(\frac{\partial p}{\partial \rho}\right)_T \leq \left(\frac{h}{\Delta t}\right)^2 + \theta.$$

IV. HEAT TRANSPORT

The evolution equation for the internal energy per unit volume E is

$$\frac{\partial E}{\partial t} + \nabla \cdot (\mathbf{u}E) = \frac{p}{\rho} \frac{d\rho}{dt} + \nabla \cdot (\lambda \nabla T) + \hat{\sigma} : \nabla \mathbf{u}, \quad (10)$$

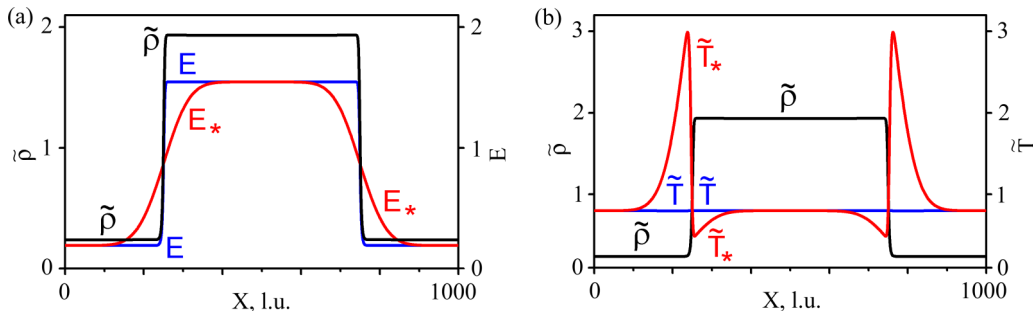


FIG. 2. Stationary 1D droplet in saturated vapor. Parasitic diffusion (spreading) of energy at phase boundaries without the use of “pseudoforces.”

where the first term on the right-hand side corresponds to the pressure work, the second term represents the heat conduction, and the last term is the viscous heating. Here, $\lambda = \rho C_V \chi$ is the heat conductivity, C_V is the specific heat at constant volume, χ is the thermal diffusivity, and $\hat{\sigma}$ is the viscous stress tensor. It is more convenient to express the pressure work through the velocity divergence

$$\frac{p}{\rho} \frac{d\rho}{dt} = -p \operatorname{div}(\mathbf{u}^*) \quad (11)$$

using the continuity equation. The viscous heating is usually small, and we neglect it in the following. The calculation of the advection of the internal energy by the fluid flow [left-hand side of Eq. (10)] with the velocity calculated from Eq. (5) is the most complicated.

The first approach proposed in Refs. [15–18] is the use of an extended set of velocity vectors \mathbf{c}_k and an increased expansion order of equilibrium distribution functions (terms up to fourth order in \mathbf{u} were used). The drawbacks of this approach are the relatively narrow range of simulated temperatures in which simulations are stable and the significant increase in the amount of data.

In Ref. [19], the advection of energy in Eq. (10) was calculated by an Eulerian finite-difference method (second approach) using values of the fluid density and velocity obtained from the LBE. However, this method produces large numerical diffusion and dispersion of energy near phase boundaries in simulations of moving fluids, which significantly complicates modeling.

The third method is based on the idea that heat is transferred to neighboring nodes in accordance with the portion of “LBE particles” that moves in this direction.

The fourth approach to simulation of the advection of energy in the LBM is based on the use of a passive scalar (additional set of distribution functions g_k such as $E = \sum_{k=0}^b g_k$) [20], which has much lower scheme diffusion compared to Eulerian finite-difference methods. Earlier, this approach was used for simulating flows with an almost-constant fluid density and specific heat where the temperature can be used as the passive scalar. At phase transitions between liquid and vapor, the change in density is, however, not small, and the advection of internal energy should be considered instead of the temperature.

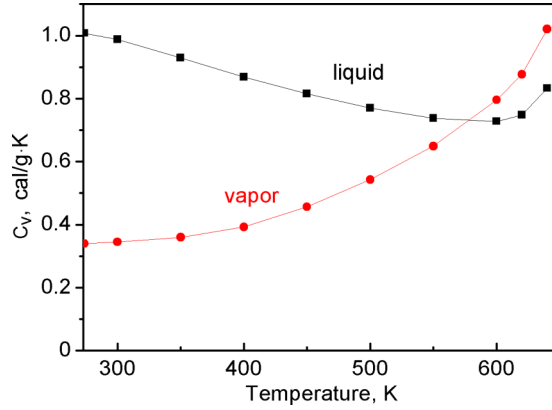


FIG. 3. Specific heat of water and vapor near the saturation curve [43].

The latter three methods were compared for some passive scalar that should move with the fluid of constant density in [22]. For simplicity, 1D uniform flow was considered. The results of simulations for velocity $u = 0.1h/\Delta t$ are shown in Fig. 1. The numerical diffusivity of the second group of methods (finite differences) is proportional to $D_1 = |u|(h/\Delta t - |u|)/2$, which depends on the fluid velocity u . The maximal value $h^2/8\Delta t$ is achieved at $|u| = h/2\Delta t$. The method of “LBE particles” has the numerical diffusivity $D_2 = h^2/6\Delta t$. For the fourth method (passive scalar), the numerical diffusivity is equal to $D_3 = (\tau_E - 1/2)h^2/3\Delta t$. In this case, the diffusivity depends on the relaxation time and can be made sufficiently low if the value of τ_E is close to $1/2$ (Fig. 1).

The passive scalar method for the LBM is usually used for single-phase flows. However, for multiphase flows, except for numerical diffusivity there exists parasitic dispersion (spreading) of energy at liquid-vapor interfaces [30]. In Ref. [31], Li and Luo proposed in 2014 that this effect is related to the internal forces introduced in the “pseudopotential” LBE method to describe phase transitions. To eliminate the unwanted effect of the forcing term on the energy equation, they introduced the

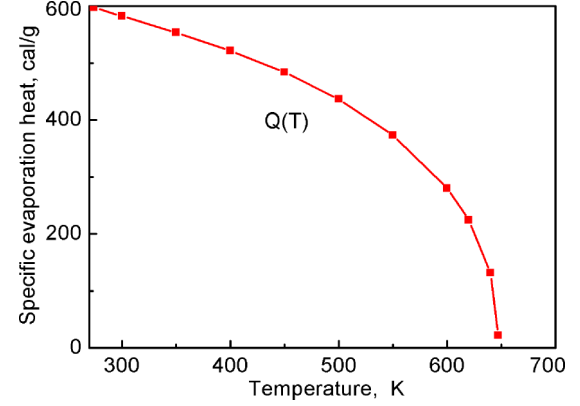


FIG. 4. Temperature dependence of the latent heat of evaporation of water [43].

correction term

$$\Delta g_k = \left(1 - \frac{1}{2\tau_E}\right) w_k C_V T \frac{(\mathbf{c}_k \cdot \mathbf{F})}{\theta} \Delta t \quad (12)$$

for distribution functions into the evolution equation

$$\begin{aligned} g_k(\mathbf{x} + \mathbf{c}_k \Delta t, t + \Delta t) \\ = g_k(\mathbf{x}, t) + \frac{g_k^{\text{eq}}(E, \mathbf{u}) - g_k(\mathbf{x}, t)}{\tau_E} + \Delta g_k(\mathbf{x}, t), \end{aligned} \quad (13)$$

which has a form analogous to Eq. (1). Here, τ_E is the nondimensional relaxation time for the energy. Equilibrium distribution functions $g_k^{\text{eq}}(E, \mathbf{u})$ have the same form as $N_k^{\text{eq}}(\rho, \mathbf{u})$ (2).

Formula (12) is similar to the part of the method of Guo *et al.* [42] for incorporation of the body force term into the LBM,

$$\Delta f_k = \left(1 - \frac{1}{2\tau_E}\right) w_k \left(\frac{\mathbf{c}_k - \mathbf{u}^*}{\theta} + \frac{(\mathbf{c}_k \cdot \mathbf{u}^*)}{2\theta^2} \mathbf{c}_k \right) \cdot \mathbf{F} \Delta t, \quad (14)$$

if one takes $\mathbf{u}^* = 0$. Here, $\mathbf{u}^* = \mathbf{u} + \Delta \mathbf{u}/2$ is the fluid velocity and $\Delta \mathbf{u} = \mathbf{F} \Delta t / \rho$ is the velocity change due to the action of internal forces at the interface during a time step. As one can suppose, formula (12) should in fact be a very crude

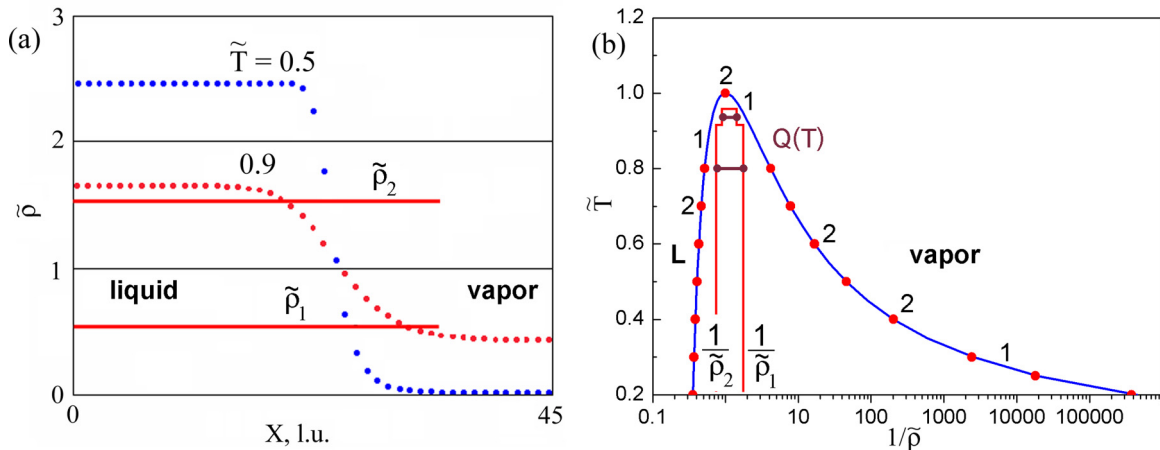


FIG. 5. Method of taking into account the latent heat of the phase transition. (a) Change in the fluid density inside the transition layers between liquid and vapor. (b) Curve 1 represents the theoretical values of the coexistence densities; points 2 are the results of LB simulations.

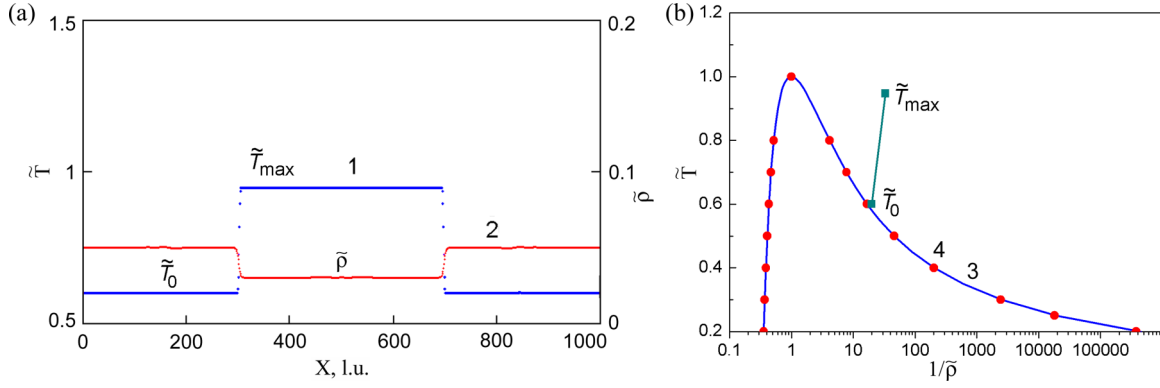


FIG. 6. (a) Initial-state distribution of the temperature (curve 1) and density (curve 2). (b) Phase coexistence curve: theoretical calculations by Maxwell rule (curve 3) and LBM simulation results (points 4). $\tilde{T}_0 = 0.6$, $\tilde{\rho}_0 = 0.05$, $\tilde{T}_{\max} = 0.947$.

approximation and it is not suitable for moving fluids where $\mathbf{u} \neq \mathbf{0}$.

We use the passive scalar approach for the internal energy density $E = \rho C_V T$. The total change in distribution functions in Eq. (13) consists of two parts, $\Delta g_k = \Delta g_k^{(1)} + \Delta g_k^{(2)}$.

The change of energy at a node ΔE due to the pressure work and the heat conduction is calculated by the usual finite-difference formulas. The release or absorption of the latent heat of evaporation is also included in ΔE (see Sec. V). Corresponding changes in energy distribution functions $\Delta g_k^{(1)}$

are proportional to the change of energy

$$\Delta g_k^{(1)}(\mathbf{x}, t) = g_k(\mathbf{x}, t) \frac{\Delta E}{E}. \quad (15)$$

The main problem with this approach stems from the jump in the specific heat per unit volume ρC_V at phase boundaries. This leads to parasitic diffusion (spreading) of the internal energy from a dense phase (liquid) to a rarefied one (vapor) even if the pressure and temperature are uniform. This effect is readily observed for stationary droplets in the case of a

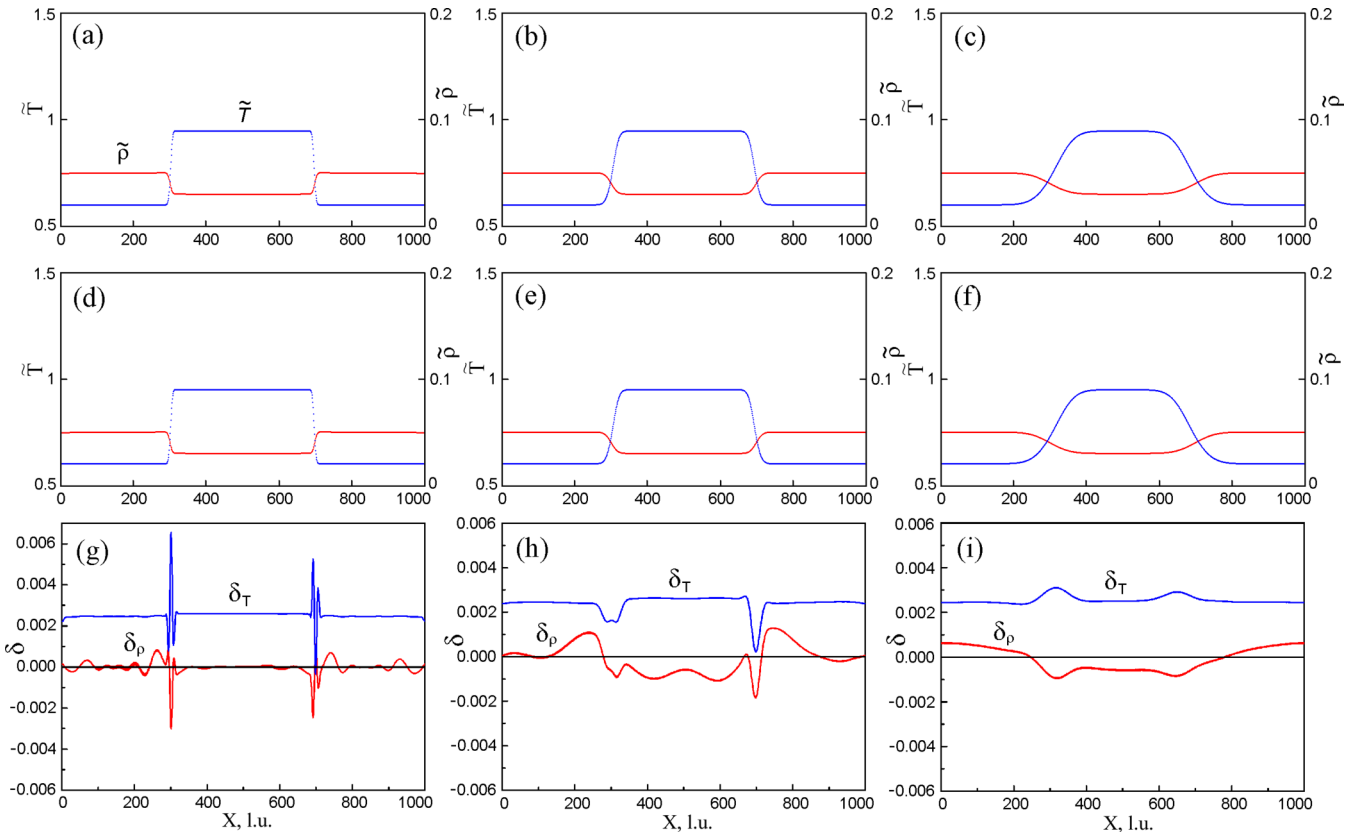


FIG. 7. Scheme diffusion of energy for flow velocities $u = 0$ (a–c) and $u = 0.1h/\Delta t$ (d–f) and relative errors (g–i) for temperature δ_T and density δ_ρ . Time $t = 10\,000$ (a, d, g), $t = 100\,000$ (b, e, h), and $t = 1\,000\,000$ (c, f, i).

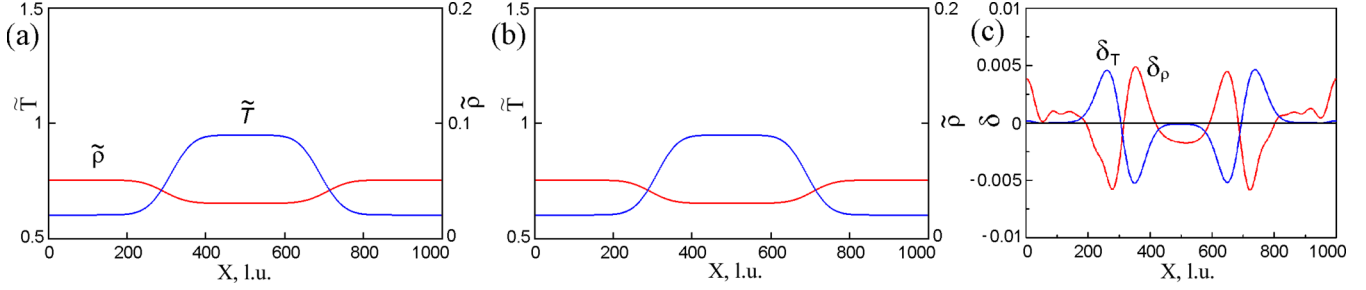


FIG. 8. (a) Thermal diffusivity $\chi = 0.01h^2/\Delta t$, $t = 100\,000$; (b) thermal diffusivity $\chi = 0.1h^2/\Delta t$, $t = 10\,000$; (c) relative differences in temperature δ_T and density δ_ρ .

barotropic equation of state (pressure depends only on density). To demonstrate the parasitic spreading of energy, the barotropic van der Waals equation of state was used with a constant temperature \tilde{T}_0 ,

$$\tilde{p} = \frac{8\tilde{\rho}\tilde{T}_0}{3 - \tilde{\rho}} - 3\tilde{\rho}^2.$$

Note that there is no feedback on temperature, hence, waves of pressure and density do not arise.

Parasitic diffusion at phase boundaries is shown in Fig. 2. The pressure work and heat diffusion are switched off for clarity. Internal energy “leaks” from the stationary liquid droplet to the surrounding saturated vapor. This leads to the generation of nonphysical temperature peaks in vapor and drops in liquid near the boundaries. In thermal simulations, such peaks and drops will lead to nonphysical waves, and the following calculations will be incorrect.

To solve this problem in the LBM, we propose considerable modification of the passive scalar approach so that it can be used for the advection of internal energy. The idea is to introduce special “pseudoforces” for the energy scalar which prevent spreading at phase boundaries. “Pseudoforces” are taken into account in the evolution equation for distribution functions, (13), in the form

$$\Delta g_k^{(2)}(\mathbf{x}, t) = g_k^{\text{eq}}(E, \mathbf{u} + \Delta\mathbf{u}) - g_k^{\text{eq}}(E, \mathbf{u}), \quad (16)$$

which is similar to the exact difference method, Eq. (3). Here, \mathbf{u} is the fluid velocity defined by the main set of lattice Boltzmann distribution functions, (4).

The currently realized variant works in the case of a constant specific heat of fluid C_V , and the internal energy at a given temperature is proportional to the fluid density. This is valid

for van der Waals and all other equations of state that are linear in temperature since for them

$$\left(\frac{\partial E}{\partial V}\right)_T = T\left(\frac{\partial p}{\partial T}\right)_V - p = 0.$$

For water, the liquid and vapor specific heats along the coexistence curve are also close in a certain range of temperatures (see Fig. 3).

V. LATENT HEAT OF THE PHASE TRANSITION

It is known that the latent heat of the phase transition should be taken into account under the conditions at a moving phase boundary. Corresponding boundary conditions are

$$\lambda_{\text{liq}} \frac{\partial T}{\partial x} \Big|_{x=\xi-0} - \lambda_{\text{vap}} \frac{\partial T}{\partial x} \Big|_{x=\xi+0} = \rho_{\text{liq}}(T) Q(T) \frac{d\xi}{dt},$$

where ξ is the coordinate of a planar phase boundary between liquid and vapor in the frame of reference of the liquid, and $\rho_{\text{liq}}(T)$ is the liquid density at the phase coexistence curve [see Fig. 5(b)]. The latent heat of the phase transition $Q(T)$ decreases with increasing temperature and reaches 0 at the critical temperature $T = T_c$ (see Fig. 4). Tracking the phase boundaries is difficult in simulations because in many cases new boundaries can appear, and existing ones can disappear or change their topology. The advantage of the LBM is its capturing of interfaces. Phase boundaries in the LBM are represented as thin transition layers where the density continuously changes from liquid to vapor values at the phase coexistence curve. The density of a portion of fluid at a phase transition also changes continuously over time. We propose taking the latent heat into account in the following way. If

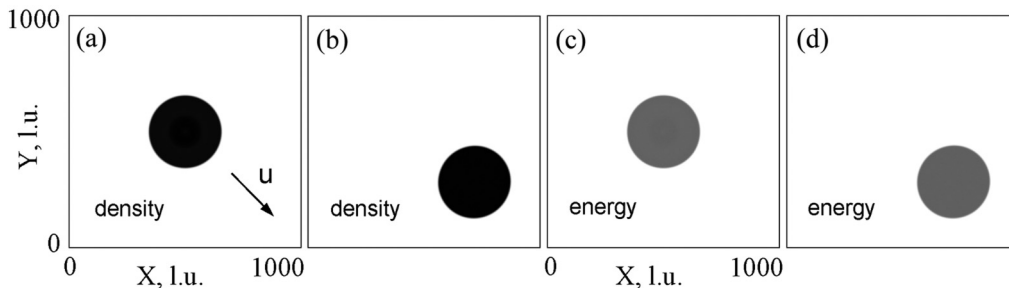


FIG. 9. Moving 2D liquid droplet of radius $R = 160$ in saturated vapor. Distribution of the density (a, b) and internal energy (c, d). Flow velocity $u_x = 0.1h/\Delta t$, $u_y = -0.1h/\Delta t$. Time $t = 0$ (a, c) and $t = 62\,000$ (b, d). Grid size, 1000×1000 .

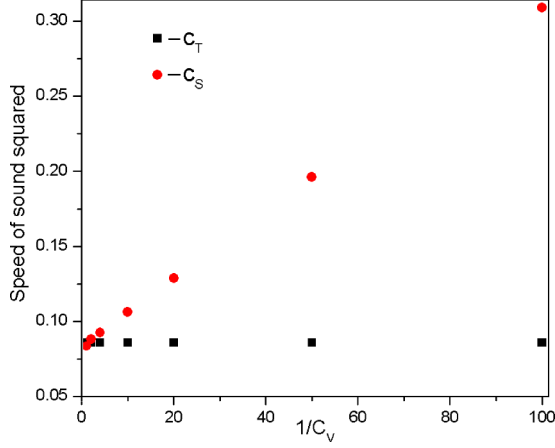


FIG. 10. Speed of sound vs inverse specific heat. Density $\bar{\rho} = 0.01$; temperature $\tilde{T} = 0.8$.

we do not want to resolve exactly the inner structure of the transition layer [see Fig. 5(a)] but take into account the latent heat of the phase transition only integrally across the transition layer, we can assume that the latent heat is released or absorbed continuously inside the transition layer in a certain range of density, $\tilde{\rho}_1 < \tilde{\rho} < \tilde{\rho}_2$, shown in Fig. 5(a) by horizontal lines $\tilde{\rho}_1$ and $\tilde{\rho}_2$. Examples of these ranges are shown in Fig. 5(b) by short horizontal lines at the temperatures $\tilde{T} = 0.8$ and $\tilde{T} = 0.94$. Hence, the corresponding energy evolution has the form

$$\frac{dE}{dt} = \frac{\rho_{\text{liq}} Q(T)}{\rho_2 - \rho_1} \frac{d\rho}{dt} = -\frac{\rho_{\text{liq}} Q(T)}{\rho_2 - \rho_1} \rho \operatorname{div}(\mathbf{u}^*). \quad (17)$$

The equilibrium densities of the vapor $\rho_{\text{vap}}(T)$ and the liquid $\rho_{\text{liq}}(T)$ at every temperature can be used as ρ_1 and ρ_2 , respectively. The temperature dependence of the evaporation heat $Q(T)$ for water [43] is shown in Fig. 4. However, in our simulations, we used a constant Q and constant values of ρ_1 and ρ_2 in a relatively narrow temperature range as the first approximation. The change in energy from Eq. (17) is included in the ΔE in Eq. (15).

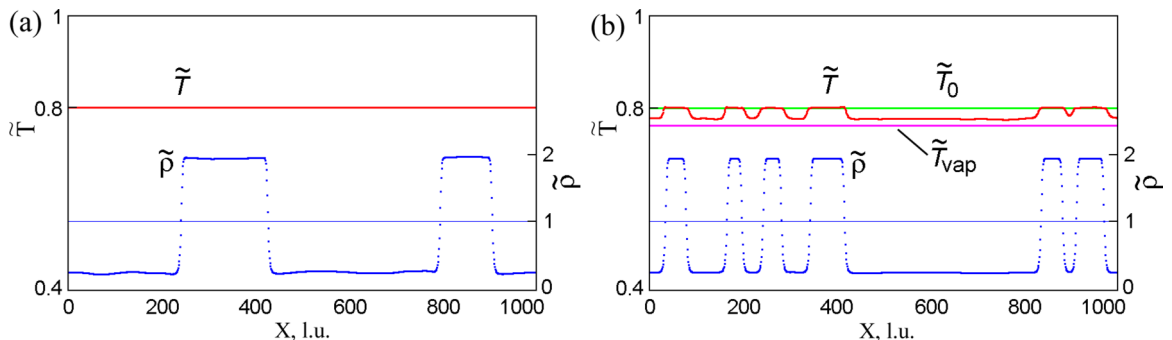


FIG. 11. Distribution of the temperature and density of the fluid after spinodal decomposition. The pressure work is neglected (a) and taken into account (b). $\tilde{T}_0 = 0.8$, $\tilde{\rho}_0 = 0.7$, $t = 50\,000$.

VI. NUMERICAL VALIDATION

A. Galilean invariance and scheme diffusion of energy

The initial state for the tests of Galilean invariance and scheme diffusion is shown in Fig. 6. The temperature and the density were distributed stepwise, and the pressure was constant. The heat conductivity was set to 0 in this simulation. Periodic boundary conditions were used. The coefficient of scheme diffusion of energy was $D_E = \theta(\tau_E - 1/2)\Delta t = 0.001h^2/\Delta t$ with $\tau_E = 0.503$.

Figure 7 shows the distribution of temperature and density at different times in the case of zero flow velocity [Figs. 7(a)–7(c)] and for uniform flow velocity equal to $u = 0.1h/\Delta t$ [Figs. 7(d)–7(f)]. Figures 7(g)–7(i) show the relative errors in density

$$\delta_\rho = \frac{\rho(u) - \rho(0)}{\rho(0)}$$

(red curves) and temperature (blue curves)

$$\delta_T = \frac{T(u) - T(0)}{T(0)}.$$

Errors are small (not larger than 0.5%). Hence, the Galilean invariance holds with a good accuracy.

Figure 8 shows the distribution of temperature in a resting fluid for two thermal diffusivities χ and corresponding times so that the product χt is equal to $1000h^2$ in both cases. The change in energy due to heat conduction $\nabla \cdot (\lambda \nabla T)$ is calculated using the usual explicit finite-difference scheme and is included in Eq. (15).

The relative differences δ_T and δ_ρ are also small (not larger than 0.5%). Hence, the similarity relation $l \sim \sqrt{\chi t}$ is fulfilled in simulations.

Since an explicit numerical scheme is used for calculating the heat diffusion, the stability criterion is $\chi \Delta t/h^2 < 0.5/d$, where d is the number of spatial dimensions. One-dimensional calculations with the flow velocity equal to $u = 0.1h/\Delta t$ and $\chi \Delta t/h^2 = 0.49$ are indeed stable.

Two-dimensional simulations are carried out using the D2Q9 model. The results are shown in Fig. 9. A round droplet surrounded by a saturated vapor moves at a uniform velocity along the diagonal of the simulation domain. Periodic boundary conditions are used for both the x and the y directions. The initial temperature is constant, hence, the density of the internal energy is higher inside the droplet. During the

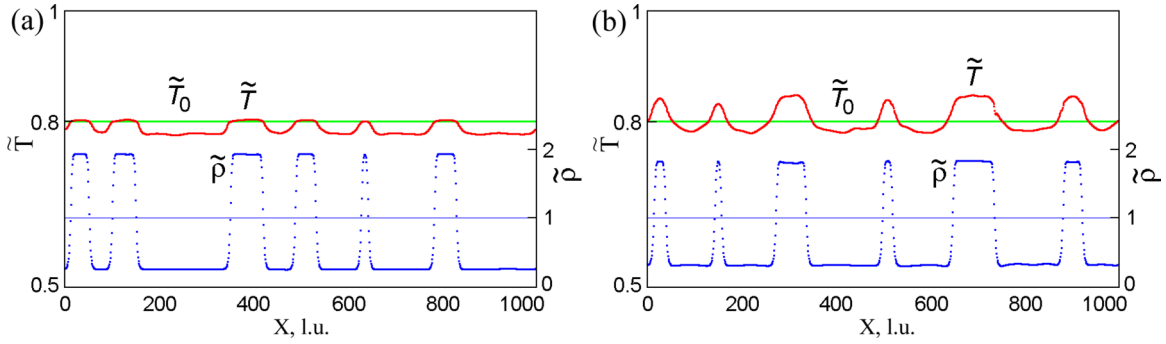


FIG. 12. Distribution of the temperature and density of the fluid after spinodal decomposition. The latent heat is $\tilde{Q} = 0$ (a) and $\tilde{Q} = 0.02$ (b). Initial temperature $\tilde{T}_0 = 0.8$, $\tilde{\rho}_0 = 0.7$, $t = 50\,000$.

simulation time of $t = 62\,000$, the droplet makes more than six revolutions together with the flow, which corresponds to 27 droplet diameters. The isotropy is preserved (the droplet remains round), and almost no parasitic diffusion of energy is present. Three-dimensional simulations with the D3Q19 model give the same results (not shown).

B. Pressure work

The pressure work was calculated using the finite-difference approximation of Eq. (11), which, in the 1D case, has the form

$$\Delta E_i^n = -p_i^n \frac{(u^*)_{i+1}^n - (u^*)_{i-1}^n}{2h} \Delta t. \quad (18)$$

In order to check the calculations of the pressure work, we investigate the dependence of the speed of sound on the specific heat. If the pressure work is switched off, one obtains the isothermal speed of sound c_T , and taking into account the pressure work gives the adiabatic speed of sound c_S . For the van der Waals equation of state, the reduced values of both speeds at the temperature \tilde{T}_0 are

$$c_T = \left(\frac{\partial \tilde{p}}{\partial \tilde{\rho}} \right)_T = \frac{24\tilde{T}_0}{(3 - \tilde{\rho})^2} - 6\tilde{\rho},$$

$$c_S = \left(\frac{\partial \tilde{p}}{\partial \tilde{\rho}} \right)_S = \frac{24\gamma\tilde{T}_0}{(3 - \tilde{\rho})^2} - 6\tilde{\rho}. \quad (19)$$

Here, $\gamma = C_P/C_V$ is the heat capacity ratio. The speed of sound was calculated from the dispersion relation for a standing harmonic wave, $c = \omega L/2\pi$, where L is the wavelength and ω is the frequency. Figure 10 shows the dependence of the speed of sound on the inverse specific heat C_V . The isothermal speed of sound is constant, and the adiabatic speed of sound depends linearly on $1/C_V$, with agreement of the theoretical result, (19).

Another test was the simulation of a spinodal decomposition (decay of an initially uniform fluid that is in the thermodynamic state below the spinodal into a mixture of liquid and vapor). Figure 11 shows the simulation results for the case with the pressure work neglected [Fig. 11(a)] and the case with the pressure work taken into account [Fig. 11(b)]. The thermal diffusivity was set to 0, and only small scheme diffusion was present. Without the pressure work, the temperature remains constant. The pressure work results in an increase

in the internal energy in the liquid phase (which arises after compression) and a decrease in the internal energy in the gas phase (where rarefaction occurs). Since the compression of liquid is relatively low, and the specific heat is significantly higher than that of the vapor, the temperature of the liquid increases only slightly. In contrast, the temperature of the gas phase decreases significantly. One can estimate the change in the vapor temperature as

$$T_{\text{vap}} = T_0 - \frac{p}{C_V} \left(\frac{1}{\rho_{\text{vap}}} - \frac{1}{\rho_0} \right).$$

The simulations give close values of the vapor temperature [Fig. 11(b)].

C. Latent heat of the phase transition

The case of spinodal decomposition was simulated with zero and nonzero latent heats of the phase transition. Results are shown in Fig. 12. When the latent heat is nonzero, the temperature of the liquid phase is significantly higher than the initial one due to the release of latent heat upon the condensation of vapor.

The 2D spinodal decomposition was simulated taking into account the pressure work and the latent heat of the phase transition. The initial uniform fluid density was $\tilde{\rho}_0 = 1$, and the temperature was everywhere $\tilde{T}_0 = 0.8$. Simulation results are shown in Fig. 13. The temperature of vapor decreased to $\tilde{T}_v \approx 0.77$, which is lower than the initial one, and the temperature

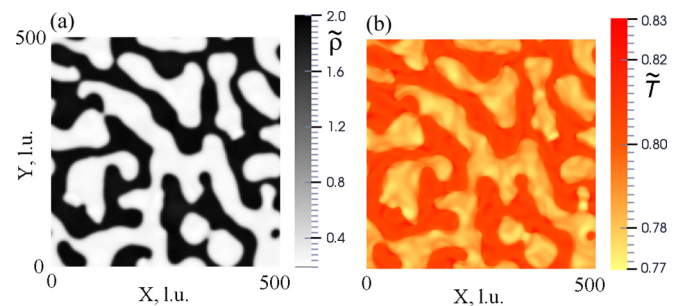


FIG. 13. Spinodal decomposition. Distribution of the density (a) and temperature (b). $\tilde{T}_0 = 0.8$, $\tilde{\rho}_0 = 1$, $\tilde{\rho}_{\text{liq}}\tilde{Q} = 0.02$. Grid size, 500×500 , $t = 2630$.

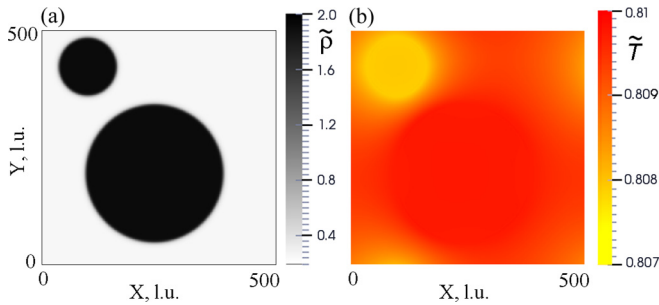


FIG. 14. Distribution of the density (a) and temperature (b) at the late stage of spinodal decomposition. $\tilde{T}_0 = 0.8$, $\tilde{\rho}_0 = 0.8$, $\tilde{\rho}_{\text{liq}}\tilde{Q} = 0.02$. Grid size, 500×500 ; $t = 1\,750\,000$.

of liquid reached the value $\tilde{T}_l \approx 0.83$, which is higher than the initial one due to the release of latent heat upon condensation.

In further evolution of the system, the number of droplets decreases due to the coalescence and evaporation of smaller droplets and the growth of larger ones. The distribution of temperature tends to a uniform one due to heat conductivity. Figure 14 shows the stage when only two droplets remain. The temperature of the smaller droplet is lower due to evaporation; the larger droplet is heated due to condensation. The temperature difference is $\Delta\tilde{T} \approx 0.01$. When the process ends and only one droplet remains, the nonuniformity of the temperature decreases to $\Delta\tilde{T} < 0.001$.

VII. CONCLUSION

The new method of an additional LB component is developed for multiphase thermal flows. The algorithm takes into account the heat conduction, pressure work, and latent heat of the phase transition. The method is interface capturing; no tracking of the phase boundaries and the conditions at them is needed. Numerical tests show that the results for a fluid at rest and a moving fluid coincide with an accuracy of better than 0.5%; hence, Galilean invariance holds for the method. Parasitic heat diffusion near boundaries with a large density gradient is suppressed by using special “pseudoforces” which prevent the spreading of energy. Two-dimensional calculations show a good isotropy. The behavior of the sound speed obtained in simulations agrees well with theoretical predictions; hence, the pressure work is taken into account accurately, which is also demonstrated in the cooling of the vapor phase during spinodal decomposition. The latent heat of the phase transition was assumed to be constant in a relatively narrow temperature range as the first approximation. The method developed is applicable for simulating flows with heat and mass transport and phase transitions for high density ratios of liquid and vapor phases.

ACKNOWLEDGMENTS

Theoretical results of this work were developed within a State task (Project No. III.22.3.1). Numerical validations were supported by the Russian Science Foundation (Grant No. 16-19-10229).

- [1] G. McNamara and G. Zanetti, Use of the Boltzmann Equation to Simulate Lattice-Gas Automata, *Phys. Rev. Lett.* **61**, 2332 (1988).
- [2] F. J. Higuera and J. Jiménez, Boltzmann approach to lattice gas simulation, *Europhys. Lett.* **9**, 663 (1989).
- [3] S. Chen and G. Doolen, Lattice Boltzmann method for fluid flows, *Annu. Rev. Fluid Mech.* **30**, 329 (1998).
- [4] C. K. Aidun and J. R. Clausen, Lattice-Boltzmann method for complex flows, *Annu. Rev. Fluid Mech.* **42**, 439 (2010).
- [5] X. Shan and H. Chen, Lattice Boltzmann model for simulating flows with multiple phases and components, *Phys. Rev. E* **47**, 1815 (1993).
- [6] Y. H. Qian and S. Chen, Finite size effects in lattice-BGK models, *Int. J. Mod. Phys. C Phys. Comput. C* **8**, 763 (1997).
- [7] A. L. Kupershtokh and D. A. Medvedev, Anisotropic instability of a dielectric liquid in a strong uniform electric field: Decay into a two-phase system of vapor filaments in a liquid, *Phys. Rev. E* **74**, 021505 (2006).
- [8] A. L. Kupershtokh, Three-dimensional simulations of two-phase liquid-vapor systems on GPU using the lattice Boltzmann method, *Numer. Methods Program.* **13**, 130 (2012) [in Russian].
- [9] A. L. Kupershtokh, Three-dimensional LBE simulations on hybrid GPU-clusters of the decay of a binary mixture of liquid dielectrics with a solute gas to a system of gas-vapor channels, *Numer. Methods Program.* **13**, 384 (2012) [in Russian].
- [10] A. L. Kupershtokh, Three-dimensional LBE simulations of a decay of liquid dielectrics with a solute gas into the system of gas-vapor channels under the action of strong electric fields, *Comput. Math. Appl.* **67**, 340 (2014).
- [11] W. Li, X. Wei, and A. Kaufman, Implementing lattice Boltzmann computations on graphics hardware, *Visual Comput.* **19**, 444 (2003).
- [12] J. Tölke and M. Krafczyk, TeraFLOP computing on a desktop PC, *Int. J. Comput. Fluid Dynam.* **22**, 443 (2008).
- [13] C. Obrecht, F. Kuznik, B. Tourancheau, and J.-J. Roux, A new approach to the lattice Boltzmann method for graphics processing units, *Comput. Math. Appl.* **61**, 3628 (2011).
- [14] S. D. C. Walsh and M. O. Saar, Developing extensible lattice-Boltzmann simulators for general-purpose graphics-processing units, *Commun. Comput. Phys.* **13**, 867 (2013).
- [15] F. J. Alexander, S. Chen, and J. D. Sterling, Lattice Boltzmann thermohydrodynamics, *Phys. Rev. E* **47**, R2249 (1993).
- [16] Y. H. Qian, Simulating thermohydrodynamics with lattice BGK models, *J. Sci. Comput.* **8**, 231 (1993).
- [17] Y. Chen, H. Ohashi, and M. Akiyama, Thermal lattice Bhatnagar-Gross-Krook model without nonlinear deviations in macrodynamical equations, *Phys. Rev. E* **50**, 2776 (1994).
- [18] A. Renda, G. Bella, S. Succi, and I. V. Karlin, Thermohydrodynamic lattice BGK schemes with non-perturbative equilibria, *Europhys. Lett.* **41**, 279 (1998).
- [19] R. Zhang and H. Chen, Lattice Boltzmann method for simulations of liquid-vapor thermal flows, *Phys. Rev. E* **67**, 066711 (2003).

- [20] X. Shan, Simulation of Rayleigh-Bénard convection using a lattice Boltzmann method, *Phys. Rev. E* **55**, 2780 (1997).
- [21] X. He, S. Chen, and G. D. Doolen, A novel thermal model for the lattice Boltzmann method in incompressible limit, *J. Comput. Phys.* **146**, 282 (1998).
- [22] D. A. Medvedev and A. L. Kupershtokh, Modeling of electrohydrodynamic flows and micro-bubbles generation in dielectric liquid by lattice Boltzmann equation method, in *Proceedings, 14th International Conference on Dielectric Liquids, Graz, Austria, 2992* (2002), pp. 45–48.
- [23] D. L. Albernaz, M. Do-Quang, and G. Amberg, Lattice Boltzmann method for the evaporation of a suspended liquid, *Interfac. Phenom. Heat Transfer* **1**, 245 (2013).
- [24] I. Rasin, W. Miller, and S. Succi, Phase-field lattice kinetic scheme for the numerical simulation of dendritic growth, *Phys. Rev. E* **72**, 066705 (2005).
- [25] D. Medvedev and K. Kassner, Lattice-Boltzmann scheme for crystal growth in external flows, *Phys. Rev. E* **72**, 056703 (2005).
- [26] A. A. Rabienataj Darzi, M. Fahradi, and M. Jourabian, Lattice Boltzmann simulation of heat transfer enhancement during melting by using nanoparticles, *IJST Trans. Mech. Eng.* **37**, 23 (2013).
- [27] A. M. Ibrahim, M. F. El-Amin, A. A. Mohammadein, and Rama Subba Reddy Gorla, Lattice Boltzmann technique for heat transport phenomena coupled with melting process, *Heat Mass Transfer* **53**, 213 (2017).
- [28] Z. Guo, C. Zheng, B. Shi, and T. S. Zhao, Thermal lattice Boltzmann equation for low Mach number flows: Decoupling model, *Phys. Rev. E* **75**, 036704 (2007).
- [29] Q. Li, Y. L. He, Y. Wang, and W. Q. Tao, Coupled double-distribution-function lattice Boltzmann method for the compressible Navier-Stokes equations, *Phys. Rev. E* **76**, 056705 (2007).
- [30] D. A. Medvedev, A. L. Kupershtokh, and I. I. Gribanov, Thermal lattice Boltzmann method for multiphase flows, in *Proceedings, 23th International Conference on Discrete Simulation of Fluid Dynamics (DSFD), Paris, France, 2014* (2014), p. 71.
- [31] Q. Li and K. H. Luo, Effect of the forcing term in the pseudopotential lattice Boltzmann modeling of thermal flows, *Phys. Rev. E* **89**, 053022 (2014).
- [32] Y. H. Qian, D. d’Humières, and P. Lallemand, Lattice BGK models for Navier-Stokes equation, *Europhys. Lett.* **17**, 479 (1992).
- [33] P. Lallemand and L.-S. Luo, Theory of the lattice Boltzmann method: Dispersion, dissipation Galilean invariance and stability, *Phys. Rev. E* **61**, 6546 (2000).
- [34] J. M. V. A. Koelman, A simple lattice Boltzmann scheme for Navier-Stokes fluid flow, *Europhys. Lett.* **15**, 603 (1991).
- [35] A. L. Kupershtokh, New method of incorporating a body force term into the lattice Boltzmann equation, in *Proceedings, 5th International EHD Workshop, Poitiers, France, 2004* (University of Poitiers, Poitiers, 2004), pp. 241–246.
- [36] A. L. Kupershtokh, Criterion of numerical instability of liquid state in LBE simulations, *Comput. Math. Appl.* **59**, 2236 (2010).
- [37] I. Ginzburg and P. M. Adler, Boundary flow condition analysis for the three-dimensional lattice Boltzmann model, *J. Phys. II France* **4**, 191 (1994).
- [38] A. L. Kupershtokh, Simulation of flows with liquid-vapor interfaces by the lattice Boltzmann method, *Vestnik NGU (Q. J. Novosibirsk State Univ.), Math. Mech. Informat.* **5**, 29 (2005) [in Russian].
- [39] A. L. Kupershtokh, C. Stamatelatos, and D. P. Agoris, Stochastic model of partial discharge activity in liquid and solid dielectrics, in *Proceedings, IEEE 15th International Conference on Dielectric Liquids, Coimbra, Portugal, 2005* (University of Coimbra, Coimbra, 2005), pp. 135–138.
- [40] A. L. Kupershtokh, D. A. Medvedev, and D. I. Karpov, On equations of state in a lattice Boltzmann method, *Comput. Math. Appl.* **58**, 965 (2009).
- [41] A. L. Kupershtokh, A lattice Boltzmann equation method for real fluids with the equation of state known in tabular form only in regions of liquid and vapor phases, *Comput. Math. Appl.* **61**, 3537 (2011).
- [42] Z. Guo, C. Zheng, and B. Shi, Discrete lattice effects on the forcing term in the lattice Boltzmann method, *Phys. Rev. E* **65**, 046308 (2002).
- [43] International Association for the Properties of Water and Steam (IAPWS) Data, Watersteampro: <http://www.wsp.ru/en/>.